Available online at www.sciencedirect.com

ScienceDirect

journal homepage: www.elsevier.com/locate/he

Green hydrogen production using doped Fe_2O_3 foams

M. Damizia [a], P.J. Lloreda-Jurado [b], P. De Filippis [a], B. de Caprariis [a], E. Chicardi [c], R. Sepúlveda [c,*]

[a] Department of Chemical Engineering Materials Environment, Sapienza University of Rome, Via Eudossiana 18, 00184, Rome, Italy

[b] Instituto de Ciencia de Materiales de Sevilla (CSIC-Univ. Sevilla), Avda. Américo Vespucio 49, 41092 Sevilla, Spain

[c] Departamento de Ingeniería y Ciencia de los Materiales y del Transporte, E.T.S. de Ingenieros, Universidad de Sevilla, Avda. Camino de Los Descubrimientos S/n., 41092 Sevilla, Spain

HIGHLIGHTS

- Green hydrogen was successfully obtained by redox process of a hematite foam.
- A hematite foam was able to deliver 5.1 $mmol H_2 \cdot g^{-1}_{sample}$ of highly pure hydrogen.
- PEM-fuel cells can be fed directly with this green hydrogen.

GRAPHICAL ABSTRACT

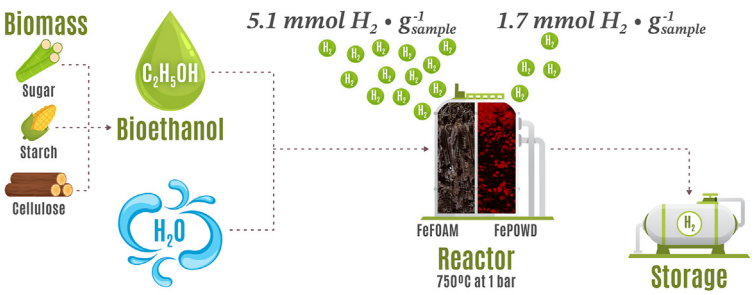

ARTICLE INFO

Article history:
Received 11 May 2023
Received in revised form
11 August 2023
Accepted 1 September 2023
Available online xxx

Keywords:
Pure hydrogen
Chemical looping
PEM fuel cell
Fe_2O_3 foams
Freeze-casting

ABSTRACT

Hydrogen is the ideal energy vector to reduce our fossil-fuels dependency and diminish the climate change consequence. However, current production is still methane based. It is possible to produce hydrogen using bioethanol from the alcoholic fermentation of organic waste by chemical looping processes, but unfortunately current redox systems generate hydrogen with significant traces of CO. In the case of proton exchange membrane fuel cells (PEMFC), hydrogen must be highly purified to produce electricity. Here, high porosity interconnected Fe_2O_3 foams doped with 2 wt% Al_2O_3 were manufactured by the freeze-casting method, obtaining around 5.1 $mmol\, H_2 \cdot g^{-1}_{sample}$ of highly pure hydrogen (<10 *ppm* of CO) consuming only 3.42 *mmol* of ethanol on each redox cycles, with no deactivation. This result shows the possibility of using an abundant and inexpensive raw material as the iron oxide to scale-up the direct pure H_2 production and facilitates its use in the automotive sector.

* *Corresponding author.*
E-mail address: rsepulveda@us.es (R. Sepúlveda).

https://doi.org/10.1016/j.ijhydene.2023.09.008

1. Introduction

Reduction of greenhouse gases emissions is our worldwide top priority demand. Sustainable Development Goal 13 encourages a 45% reduction for the next decade with net zero emissions target by 2050. This situation leads to an urgent change in our main energy sources: hydrogen is the most promising new energy vector because it does not produce CO_2 and its energy content per unit of weight is three times that of gasoline. However, hydrogen production is far from environmentally friendly; today, 60% of H_2 production uses methane gas as the main source, resulting globally in 900 Mt of CO_2 emissions per year [1]. Currently, new methods of production are being tested, implemented, or scaled, such as the electrolysis of water by solar [2], wind [3], or fusion energy [4], as they use renewable energy sources to break the water molecule and release hydrogen; this will produce the so-called green hydrogen.

Another possibility is to use a chemical looping method based on the redox behaviour of iron oxides to obtain green hydrogen; in a typical chemical looping hydrogen process, iron oxides are first reduced by a renewable gaseous/solid reductant and later, iron is oxidized by steam to produce H_2, this is known as the steam iron process (SIP). As Fe own several oxidation states available, the reduction of iron oxides to metallic Fe and subsequent Fe oxidation occurs by numerous reactions. The list of the main reactions occurring in the presents of H_2, CO or solid C as reductants and steam as oxidizing agent are reported below (eqs. (1)–(11)) [5].

Reduction step:

$$3Fe_2O_3 + H_2 \rightleftarrows 2Fe_3O_4 + H_2O \quad \Delta H_{900^\circ C} = -7.175 kJ/mol \tag{1}$$

$$3Fe_2O_3 + CO \rightleftarrows 2Fe_3O_4 + CO_2 \quad \Delta H_{900^\circ C} = -41.09 kJ/mol \tag{2}$$

$$3Fe_2O_3 + C \rightleftarrows 2Fe_3O_4 + CO \quad \Delta H_{900^\circ C} = +50.09 kJ/mol \tag{3}$$

$$Fe_3O_4 + H_2 \rightleftarrows 3FeO + H_2O \quad \Delta H_{900^\circ C} = +50.61 kJ/mol \tag{4}$$

$$Fe_3O_4 + CO \rightleftarrows 3FeO + CO_2 \quad \Delta H_{900^\circ C} = +15.70 kJ/mol \tag{5}$$

$$Fe_3O_4 + C \rightleftarrows 3FeO + CO \quad \Delta H_{900^\circ C} = +40.61 kJ/mol \tag{6}$$

$$FeO + H_2 \rightleftarrows Fe + H_2O \quad \Delta H_{900^\circ C} = +15.03 kJ/mol \tag{7}$$

$$FeO + CO \rightleftarrows Fe + CO_2 \quad \Delta H_{900^\circ C} = -19.88 kJ/mol \tag{8}$$

$$FeO + C \rightleftarrows Fe + CO \quad \Delta H_{900^\circ C} = +30.61 kJ/mol \tag{9}$$

Steam-Oxidation step:

$$Fe + H_2O \rightleftarrows FeO + H_2 \quad \Delta H_{900^\circ C} = -95.6 kJ/mol \tag{10}$$

$$3FeO + H_2O \rightleftarrows Fe_3O_4 + 4H_2 \quad \Delta H_{900^\circ C} = -55.6 kJ/mol \tag{11}$$

Previous studies have demonstrated the potential use of this technology to reuse/revalue industrial stream gases [4,6,7] and purified hydrogen gas mixtures [8], as well as to employ biomass as a raw material to produce hydrogen [9–12]. These promising studies share a common drawback: the deactivation effect over the iron oxide particles due to the high operational temperature (600–800 °C), leading to a reduction in the porosity and the sintering of the particles [13]. Many authors have attempted to overcome this problem by changing the chemical composition of the particles by adding single oxides such as Al_2O_3 [14], MnO_2 [15], CeO_2 [16], or binary oxides [17], through different manufacturing methods such as mechanical mixing or coprecipitation.

Another approach is to replace the particles with ceramic porous materials, such as foams or scaffolds, which ensures a minimum and constant reactive surface area while reducing the sintering process. The use of such monolithic samples with tailored porosity have been demonstrated significant improvements in the catalytic process such as the methanation of syngas [18] and the water-gas shift (WGS) reaction [19] due to a combination of improved heat transfer together with a lower pressure drop. Also, improvements in the gas transportation throughout the monolith part has been established [20], as porous materials are also being also as catalysts by simply impregnating a porous template [21]. Recent studies have demonstrated the feasibility of this approach for SIP [8,22,23]. However, to enhance the efficiency of chemical looping processes, the oxide should be fully reduced to Fe, which ensures the maximum production of hydrogen but exposes the metal to ideal sintering conditions (high temperature and free oxide surfaces). Furthermore, the growing oxide scale at the oxidation step is detached from the metal base throughout the redox cycles or forms closed pores via the Kirkendall effect [22].

Chang et al. [24] suggest the use poly (ethylene oxide) (PEO) as a pore former to create a hierarchical pore structure in the iron oxide-based oxygen carrier supported with Al_2O_3. The work demonstrates the positive effect of the uniform mesoporous pore size and macroporous structure utilized, reaching a 343 ml H2/g of carrier. Ma et al. [25] add SrO to powder Fe_2O_3/Al_2O_3 oxygen carriers to prevent particle sintering (i.e. deactivation effect) during redox cycling when solid fuels are used. The addition of Sr increment the surface oxygen vacancy and adsorbed oxygen improve reactivity of the material during the CLC (chemical looping combustion) reaction.

The performance of iron oxide-based oxygen carriers doped with Al_2O_3 is strongly related with the ability of the system to avoid the segregation of Al (or Fe) atoms by solid state diffusion during redox cycling [26]. Ma et al. [27] conducted a study were nanometric particles of Fe_2O_3 and Al_2O_3 were mechanically mixing in 1:1 ratio and sintered at 1300 °C for 2h. The carriers show a clear deactivation after few cycling at all tested temperatures (700, 800 and 900 °C) mainly due to a significant surface sintering. The authors claims that higher reaction temperatures enrich the particle surface with active components, (i.e. Fe cations moving outward). However, these high operational temperatures could lead to an impervious layer of Fe/FeO that limits further reduction reactions.

Furthermore, the full reduction to iron must be avoided to prevent rapid particle sintering or pore clogging when the target product needs pure hydrogen ($CO < 10$ ppm), such the proton exchange membrane (PEM) fuel cells. In the presence of complex carbonaceous reductant (such as bioethanol, biomass, pyrolysis oil), a solid layer of carbon is formed during the reduction step catalysed by the iron/iron oxide phases [28].

Please cite this article as: Damizia M et al., Green hydrogen production using doped Fe_2O_3 foams, International Journal of Hydrogen Energy, https://doi.org/10.1016/j.ijhydene.2023.09.008

If free-oxide surface is achieved, the carbon consumption by reduction reactions is impeded and in the subsequent steam oxidation it is responsible of H_2 contamination by CO [29] (eq. (12)), a poison of the PEM-type fuel cell catalyst.

$$C + H_2O \rightleftarrows CO + H_2O \quad (12)$$

When bioethanol is selected as reducing agent, in fact, at the operative conditions required for the process it undergoes cracking reaction producing a gaseous stream mainly composed by CO, H_2 and solid carbon, according to the reactions reported below (eqs. (13) and (14)) [9]:

$$CH_3CH_2OH \rightleftarrows CO + H_2 + CH_4 \quad \Delta H = +49 kJ/mol \quad (13)$$

$$CH_4 \rightleftarrows C + 2H_2 \quad \Delta H = +74.35 kJ/mol \quad (14)$$

The control of reduction time was one of the strategies studied to limit the iron oxide reduction degree ensuring sufficient oxygen in the fixed bed; however, the optimal reduction time strongly depends on both chemical composition and morphology of the redox material, type of reductant selected and process configuration adopted.

In this work, coprecipitated Fe_2O_3 nanoparticles doped with 2 wt% Al_2O_3 were used to manufacture an interconnected porous foam by freeze-casting, suitable for the production of pure and renewable hydrogen by a chemical looping process. The foams were tested in a bench scale plant with a fixed bed reactor, using commercial bioethanol and steam as the reductant and oxidizing gas, respectively. An in-depth experimental study on the redox behaviour of Fe_2O_3-based foams and the optimization of the process parameters are fundamental to scale up the proposed technology; the highly interconnected pore structure of FeFOAM in fact gives the fixed bed reactor lower pressure drops than spherical particles. The foams (FeFOAM) were subjected to 10 redox cycles at different temperatures (675, 700, and 750 °C) and reduction time durations (3, 4, and 5 *min*) that at constant ethanol flow rate correspond to 3.42, 4.57 and 5.71 mmol of ethanol fed, respectively. The control of the reduction time has been selected as strategy to avoid the complete iron oxide reduction to Fe: by decreasing the amount of ethanol fed a lower iron oxide degree was achieved Material characterization and equal redox tests were also performed on Fe_2O_3 based particles (FePOWD) with the same chemical composition of FeFOAM for comparison.

2. Experimental procedure

2.1. Powder synthesis

To manufacture the FeFOAM first, Fe_2O_3 nanopowders doped with 2 wt% of Al_2O_3 were synthesized using the citrate method, as previously reported [30]. A 2 M metal nitrates solution of $(Fe(NO_3)_3 \cdot 9H_2O$ and $Al(NO_3)_3 \cdot 9H_2O$ was mixed and stirred at 80 °C with citric acid for about 4 *h* until complete gelatinization. The gel was then dried during a least 12 *h* at 110 °C to later calcined for 8 *h* at 620 °C. Finally, the powders were wet ball-milled for 24 *h*, dried, and manually crushed. Reagents (98% of purity or more) were purchased from Alfa Aesar™.

FePOWD powders were synthesized by coprecipitation method. Fe and Al nitrate salts were first dissolved in deionized water, a 30 vol% of aqueous ammonia solution was gradually added until a pH of 9 was obtained in the solution. The resultant precipitate was washed, filtered, and then dried at 110 °C for 24 *h*. The particles were calcined in a two-step heat treatment: 350 °C for 2 *h* followed by 2 *h* at 900 °C. Lastly, the powders of 20–150 μm in size were obtained by crushing and sieving. Reactive (98% of purity or more) were purchased from Sigma Aldrich.

2.2. FeFOAM manufacturing

The FeFOAM were manufactured according to a previous study [31]. Briefly, a 10 vol% FeFOAM powder camphene suspension was created by ball milling using 3 wt% stearic acid as a dispersant agent. The suspension was freezes cast by filling a mould of 15 *mm* in diameter by 18 *mm* in height preheated at 60 °C and directionally solidified by running tempered water through the mould base to promote the axial growth of camphene dendrites. The sample is de-moulded and camphene is sublimated under ambient conditions. Finally, a sintering process at 1100 °C for 2 *h* was applied. FeFOAMs were approximately 10 *mm* in diameter and 12 *mm* in height to fit into the quartz-tube reactor.

2.3. Redox test

Redox experiments were conducted in a lab-made quartz tube reactor (10 *mm* of inner diameter and 300 *mm* of length) heated at the desired temperature using an external electric heater. A syringe pump was employed to feed ethanol and water alternatively in the two steps of the process (reduction and oxidation). The ethanol and water flow rates were constant for all the tests and equal to 4 mL/h and they are vaporized at 230 °C before entering at the top of the reactor. All experiments were conducted in the presence of 230 mL/min of Ar as carrier gas. The operating conditions in term of gas hourly space velocity (GHSV) are maintained constant for both the sample and type of reaction ($GHSV_{red}$ = 14000 h^{-1} and $GHSV_{ox} = 19000\ h^{-1}$). During each redox cycles, the outline gas composition was determined in real-time by a Quantitative Gas Analyser (QGA) mass spectrometer from Hiden Analytical (sampling interval of 10 *s*). The CO (*ppm*) concentration was monitored by a non-dispersive infrared sensor (Comet 0005-14-312 model) from Ambra Sistemi (sampling interval of 3 *s*). The simplified scheme of the experimental set-up adopted for the tests (Fig. 1) was fully described in previous work [5].

The FeFOAM samples were designed in a cylindrical shape compatible with the reactor dimensions to avoid preferential flow regions in the fixed bed. The total weight of FeFOAM sample was about 0.50 *g*. In the case of FePOWD experiments, the fixed bed was composed of 1.00 *g* of FePODW mechanically mixed with 0.50 *g* of SiO_2 to reduce the thermal gradient in the solid bed and prevent the particle's agglomeration.

The redox performance of FeFOAM and FePOWD was evaluated under 3 different operational temperatures (675, 700, and 750 °C) and 3 reduction times (3,4 or 5 *min*). During the reduction step, ethanol was fed at a constant flow rate for 3, 4, or 5 *min*, corresponding to 3.42, 4.57, and 5.71 *mmol*, respectively. As demonstrated by the authors in previous works [5,9,32],the control of the amount of ethanol fed is a promising

Please cite this article as: Damizia M et al., Green hydrogen production using doped Fe_2O_3 foams, International Journal of Hydrogen Energy, https://doi.org/10.1016/j.ijhydene.2023.09.008

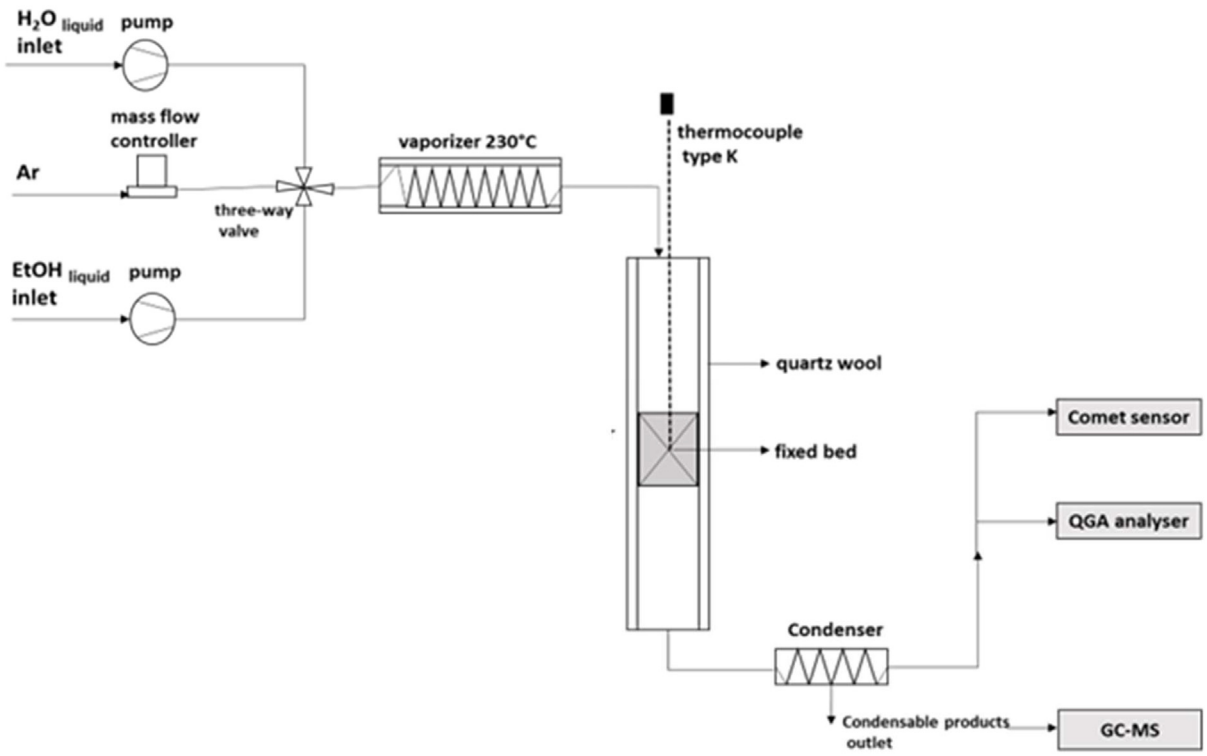

Fig. 1 – Simplified scheme of the experimental set-up.

solution to avoid the complete reduction to Fe and therefore the carbon deposition. The oxidation step was performed by flowing steam until the complete Fe oxidation. The volume of hydrogen (*mL*) produced at each oxidation state is calculated according to equation (15):

$$V_{H2} = \int_{t1}^{t2} F_{tot} * y_{H2}\, dt \tag{15}$$

where the difference between t_1 and t_2 correspond to the duration (*min*) of the oxidation step, F_{tot} is the total gaseous stream ($mL \cdot min^{-1}$) and y_{H2} is the volumetric fraction of H_2 in the gaseous stream, measured by the mass spectrometer.

The *H_2 yield* have been calculated as function of the amount of H_2 (*mmol*) per mass of sample (g_{sample}) incorporated in the reactor at each ethanol fed according to equation (16):

$$H_2\ yield = mmol\ H_2 \cdot g_{sample}^{-1} \tag{16}$$

Similar calculation has been used by others authors [33] to highlight the potential use of the ethanol as fuel to produce hydrogen. Furthermore, the Efficiency of the process (*E*) was obtained at each oxidation step according to equation (17):

$$E = \frac{V_{H_2\ experimental}}{V_{H_2\ theoretical}} \cdot 100 \tag{17}$$

where $V_{H_2\ experimental}$ is the volume of H_2 produced while $V_{H_2\ theoretical}$ is the maximum H_2 producible by the sample, if complete conversion into Fe is reaching during reduction and full oxidation to Fe_3O_4 is obtained in the presence of steam. This parameter indicates the reduction degree achieved in the iron oxides at each tested condition.

2.4. *Foam characterization*

After redox tests, the thermal stability of the FeFOAM sample was determined through Archimedes' method to obtain the variation of the total porosity (%). Samples were summered in water for 5 *min* during vacuum (10^{-2} *bar*) to fully impregnated the open porosity. Finally, FeFOAM samples were characterized by: a) X-Ray Diffraction analysis (XRD) to determine the crystal phases, b) Scanning Electron Microscopy (SEM) to determine the sample surface; and c) Transmission Electron Microscopy (TEM) to establish any element distribution or segregation.

3. Results and discussion

3.1. *Initial state of the FeFOAM and FePOWD samples*

Initially, the FeFOAM sample is a cylinder of approximately 10x12 *mm* according to Fig. 2a. At the surface, it can be observed an elongated pore structure aligned with the cooling direction applied during freeze-casting processing. The interconnected pore structure is created by the dendritic replication during camphene solidification (Fig. 2b). Pores have a diameter of 80–150 μm with a wall thickness of 4–10 μm, as previously reported [31]. The density of the FeFOAM samples were 1.3–1.4 g/cm^3 exhibiting an open porosity of 65 % obtained by Archimedes' method. The use of SA in the manufacture of FeFOAM sample induced a small reduction during sintering [30], lowering the concentration of oxygen carriers due to the formation of magnetite phase. On the

Please cite this article as: Damizia M et al., Green hydrogen production using doped Fe_2O_3 foams, International Journal of Hydrogen Energy, https://doi.org/10.1016/j.ijhydene.2023.09.008

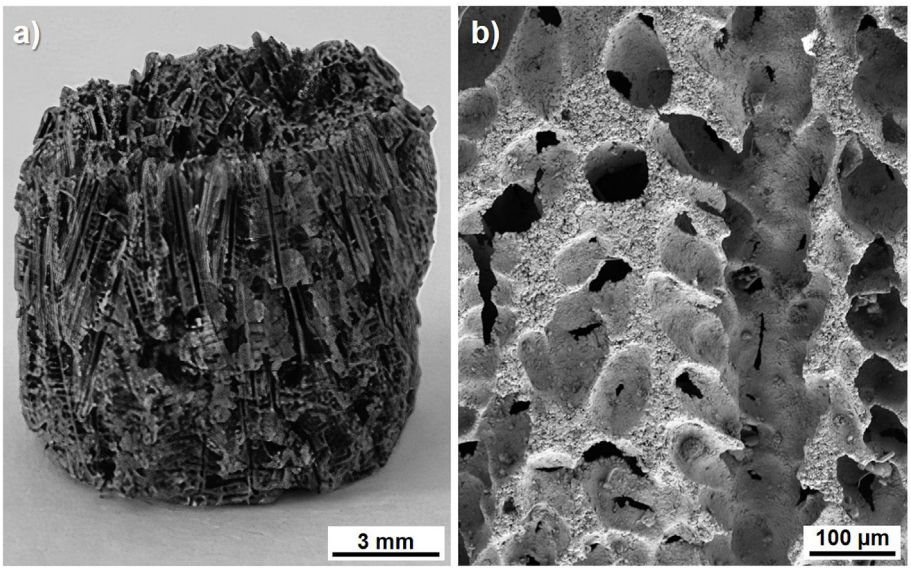

Fig. 2 – Optical image of the FeFOAM sample (a) and SEM image of the internal pore structure before redox test (b).

contrary, the FePOWD samples showed only hematite phase during XRD characterization [32].

3.2. *Redox test: operative conditions 675 °C and 1 bar*

Fig. 3 shows the H_2 *yield* (scale bar) and the maximum *CO* concentration on each redox cycle (lines) of the FeFOAM (Fig. 3a) and FePOWD (Fig. 3b) samples according to the amount of ethanol fed (3.42, 4.57, and 5.71 *mol*) at 675 °C and 1 *bar*. These results indicate that, as more ethanol was introduced into the reactor, both samples reached a deeper degree of reduction and were able to produce more hydrogen during each re-oxidation reaction. Furthermore, both Fe_2O_3-based samples showed no deactivation after 10 redox cycles confirming that the presence of 2 wt% of Al_2O_3 confers to iron a higher thermal resistance, regardless of the morphology of the sample. Based on the results, the highly interconnected porous structure of FeFOAM significantly changes the iron redox activity. During redox cycling at 675 °C, FeFOAM was able to double the H_2 *yield* values to those obtained with the FePOWD (sample FeFOAM reached up to 7.9 *mmol* $H_2 \cdot g^{-1}_{sample}$ while FEPOWD produces only 2.5 *mmol* $H_2 \cdot g^{-1}_{sample}$ at 5.71 *mmol* of ethanol fed), highlighting the higher accessibility of the iron oxide active sites by the reductant gas. This property has led to a deeper reduction degree and consequently to a more efficient oxidation.

These results show the improvement of hydrogen production due to the interconnected porosity incorporated into the oxygen carrier under the same experimental condition. In the case of particles, the maximum active surface depends on the particle diameter by ~$4\pi R^3$ (being *R* the particle radius). However, ensuring access to the entire particle surface is limited by the reactor own capacity to rise and gasify the particles completely. Moreover pore size is also important, Chang et al. [24] created a hierarchical pore structure in the iron oxide-based oxygen carrier supported with Al_2O_3 using PEO as a pore former. Hydrogen production reach 15.3

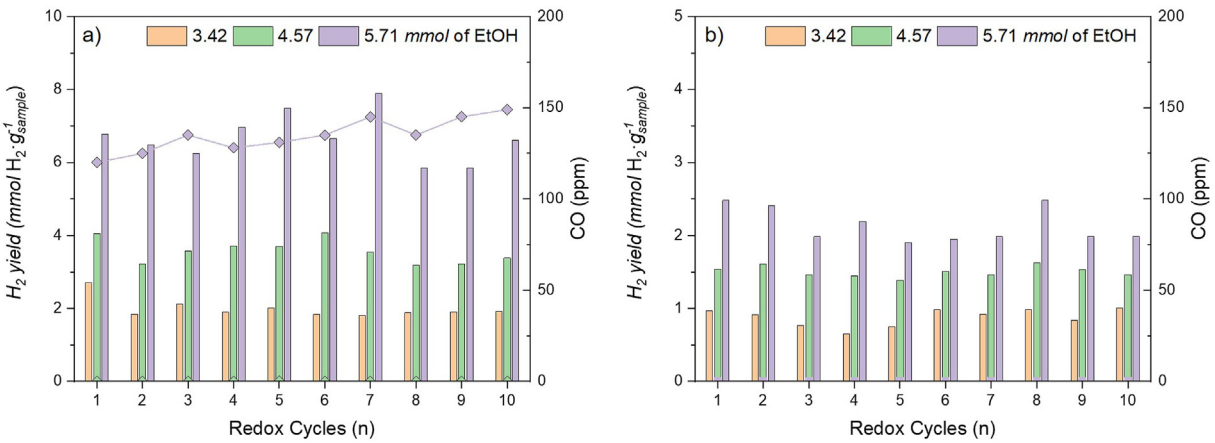

Fig. 3 – H_2 *yield* in scale bar and *CO* concentration in coloured line of FeFOAM (a) and FePOWD (b) samples at 675 °C and 1 *bar* during 10 consecutive redox cycles according to the amount of ethanol fed at the reduction reaction.

Please cite this article as: Damizia M et al., Green hydrogen production using doped Fe_2O_3 foams, International Journal of Hydrogen Energy, https://doi.org/10.1016/j.ijhydene.2023.09.008

$ml\ H_2 \cdot g^{-1}_{carrier}$ suggesting the benefits of the initial relatively large pore volume however, it drops within a few redox cycle due to the rapid reduction of the macropores below 20 μm. This impairment effect has also been observed in previous work [34,35]. In this work, the use of the freezes-casting technique allows a more efficiency use of the porosity and it redox capability on the iron-based oxygen carriers using a single method of manufacturing.

The presence of *CO* during the oxidation reaction was also monitored during redox cycling, as a measurement of the purity of the hydrogen produced. The FePOWD sample produced a hydrogen stream with a concentration of *CO* under detection limits (10 *ppm*) at any reduction conditions (Fig. 3b). However, the FeFOAM sample released about 150 *ppm* of *CO* only when the highest amount of ethanol was fed (5.71 *mmol*) (Fig. 3a), suggesting that the carbon deposition during the reduction occurs. These results show the main downside of the proposed system: the difficulty to obtain a highly pure hydrogen stream at deeper iron oxide reduction degree. The presence of *CO* in the FeFOAM sample is linked to the lower concentration of oxygen in the sample surface at the end of the reduction step, linked to the higher accessibility to the active sites than FEPOWD; this condition promotes the carbon deposition and the contamination of H_2 flow.

The enhanced performance of the FeFOAM is also visible in Fig. 4, where the average H_2 *yield* was significantly higher at all the amount of ethanol fed compared with the FePOWD sample. With 4.57 , FeFOAM showed an average H_2 *yield* about 2.3 times higher than its particle counterpart. At 5.71 *mmol* condition, the FeFOAM produced the highest average H_2 *yield* value (6.7 $mmol\ H_2 \cdot g^{-1}_{sample}$) but a contamination of 150 *ppm* of *CO* was detected, making it unusable for PEM fuel cell application. However, the H_2 flow possess a purity of 99.995% that satisfy uses of hydrogen for which the quality requirements are less stringent (i.e. combustion plants, for power and heat generation, and in aerospace applications).

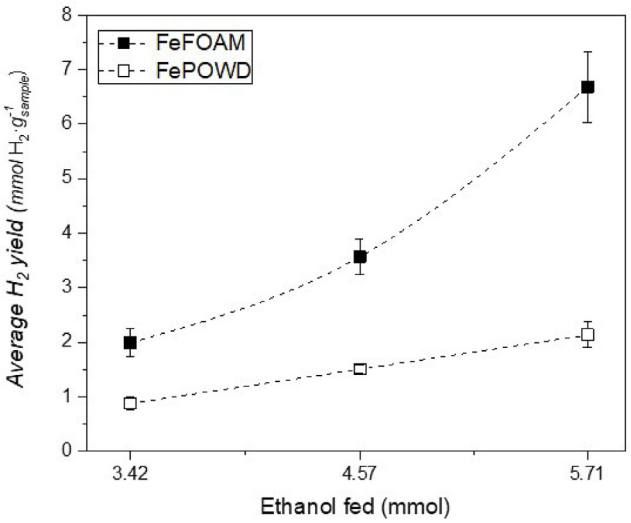

Fig. 4 – Average H_2 *yield* as a function of ethanol fed at 675 °C and 1 *bar* for FeFOAM and FePOWD samples.

3.3. *Influence of redox operative conditions in the pure H_2 production*

To understand the influence of temperature on the H_2 *yield*, and purity and to assess the thermal resistance of FeFOAM,10 consecutive redox cycles were conducted at higher temperatures (700 and 750 °C) and 1 *bar*. The increase of temperature could compromise the particle or pore structure stability due to its low thermal stability, besides of ethanol conversion into carbon and the iron oxide reduction are enhanced due to the endothermic nature of these reactions. These critical aspects could lead to a reduction of the H_2 *yield* and H_2 purity. Fig. 5 shows the H_2 *yield* (scale bar) and the maximum *CO* concentration on each redox cycle (lines) at the highest temperature of the study 750 °C, conditions for which the effect of temperature is more evident. The results of the FeFOAM and FePOWD according to the amount of ethanol fed were reported in Fig. 5a and b, respectively.

From the results collected in Fig. 5, the increase of 675 °C to 750 °C at the reaction temperature does not produce sample deactivation after 10 consecutive redox cycles, demonstrating that the improvement on the thermal resistance by the addition of Al_2O_3 in during particle synthesis. Fig. 5a shows the FeFOAM samples reaching a steady value about 12 $mmol\ H_2 \cdot g^{-1}_{sample}$ when 5.71 *mmol* of ethanol was fed, while at the same conditions sample FePOWD generated approximately 6 $mmol\ H_2 \cdot g^{-1}_{sample}$. The increase of temperature does not change the enhanced activity of FeFOAM samples, still able to raise the H_2 *yield* by almost a factor of 2 with respect the powders Again, as less ethanol is introduced into the reactor the hydrogen production diminishes.

However, at higher temperatures, the levels of *CO* increased according to the profiles reported in Fig. 5 (lines). For both samples, a decrease of the optimal ethanol value with respect the data collected at 675 °C was detected. In the test with FeFOAM (Fig. 5a) no *CO* was detected at 3.42 *mmol* of ethanol fed, but when the ethanol intake rises to 4.57 and 5.71 *mmol*, the *CO* concentration scale up to 2300 and 5000 *ppm* since the first oxidation step, respectively. This confirms the deleterious effect of the temperature over the H_2 purity when a carbonaceous reductant gas was used at higher reduction temperature. In the case of the FePOWD sample, the lower reduction degree and the higher oxygen concentration avoids the *CO* contamination at 4.57 *mmol* of ethanol fed only in the first 3 cycles, then *CO* rise significantly at cycles number 4 from a concentration of 120 *ppm* to 1000 *ppm* at 10th cycle (Fig. 5b, green line), suggesting that carbon accumulation occurs cycle after cycle. The same carbon accumulation trend is registered when 5.71 *mmol* of ethanol are fed. Based on these results, at 750 °C the optimal ethanol value for both samples was 3.42 *mmol*, in which the FeFOAM sample still own a major activity of FePOWD (5.2 and 1.5 $mmol\ H_2 \cdot g^{-1}_{sample}$ for FeFOAM and FePOWD, respectively).

The effect of the operative temperature on the H_2 *yield* is show in Fig. 6, where an evaluation of the average H_2 *yield* obtained with FeFOAM (Fig. 6a) and FePOWD (Fig. 6b) as function of the redox temperature and ethanol fed were reported. The results gathered in Fig. 6 demonstrated the key role played by temperature in the system proposed. By feeding

Please cite this article as: Damizia M et al., Green hydrogen production using doped Fe_2O_3 foams, International Journal of Hydrogen Energy, https://doi.org/10.1016/j.ijhydene.2023.09.008

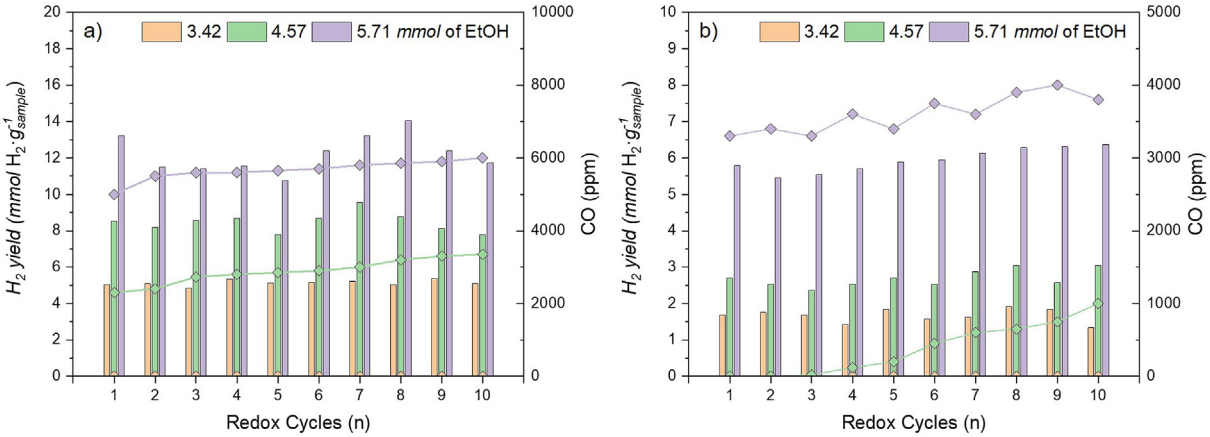

Fig. 5 – H_2 *yield* in scale bar and CO concentration in coloured line of FeFOAM (a) and FePOWD (b) samples at 750 °C and 1 *bar* during 10 consecutive redox cycles according to the amount of ethanol fed at the reduction reaction.

3.42 *mmol* of ethanol to the FeFOAM, the average H_2 *yield* value was 2 *mmol* $H_2 \cdot g^{-1}_{sample}$ while, by increasing the temperature until 750 °C, value reached 5.1 *mmol* $H_2 \cdot g^{-1}_{sample}$ with no detection of *CO* in the gas stream. The result indicate that the increase of temperature promotes the iron oxides reduction favouring at the same time the consumption of carbon during this phase. An enhanced activity was observed also for the FePOWD sample, although with a lesser extent with the temperature, when 3.42 *mmol* of ethanol was fed, the average H_2 *yield* value reached 1.7 *mmol* $H_2 \cdot g^{-1}_{sample}$ at 750 °C, almost double respect to the results obtained when the same ethanol amount at 675 °C, both with no *CO* contaminations.

From the comparison of the sample results, at 700 °C FeFOAM sample is able to produce approximately 3.7 *mmol* $H_2 \cdot g^{-1}_{sample}$ of pure H_2 when the ethanol fed was 4.57 *mmol*. More conditions with no *CO* detected were noticed for FePOWD at all ethanol fed for 675 and 700 °C but a maximum of 2.2 *mmol* $H_2 \cdot g^{-1}_{sample}$ of H_2 was obtained. At 750 °C both samples produce pure H_2 only at 3.42 *mmol* of ethanol fed. The pure hydrogen regions were highlighted by the shaded areas in Fig. 6.

The direct production of H_2 streams by chemical looping process suitable for PEM fuel cells operation using bioethanol as reducer is still not achieved in literature. Many studied are focused on the chemical looping reforming process, where a mixture of ethanol and water was fed during the reduction step instead of pure ethanol. This solution limits the issues of carbon deposition at the expense of total process costs. Trevisanut et al. [36] studied the reforming process of bioethanol using Fe_3O_4 and $NiFe_2O_4$ particles as a fixed bed, but during the reduction step the carbon deposition remains the main obstacle of the pure hydrogen production. Zeng et al. [37] achieved a hydrogen purity approximately of 96% using NiO/$MgAl_2O_4$ particle mixture in a fixed-bed reactor. As a different approach, Jiang et al. [38] prepared oxygen carriers of NiO/montmorillonite by ultrasound assisted cation exchange impregnation method, but an air oxidation step was needed to convert the deposited carbon at the end of each cycles.

The variation of process efficiency value as a function of the operative conditions studied summarized in Table 1 confirm the benefit of using a foam to achieve deeper iron oxide reduction degree; FeFOAM is always superior, reaching *E* values up to 73%. Values underlined in Table 1 shows the redox conditions were H_2 purity is neglected (*CO* over 10 *ppm*), and therefore the experimental H_2 volume produced by carbon gasification reactions should be taken into account for the

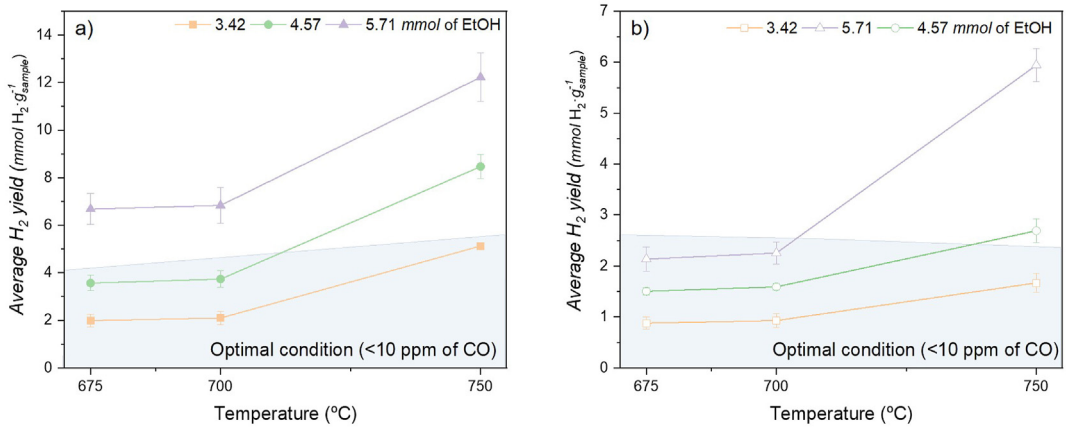

Fig. 6 – Average H_2 *yield* as a function of redox temperature and ethanol fed for FeFOAM (a) and FePOWD (b) samples. Shaded areas highlight the optimal redox condition to obtain high purity hydrogen.

Please cite this article as: Damizia M et al., Green hydrogen production using doped Fe_2O_3 foams, International Journal of Hydrogen Energy, https://doi.org/10.1016/j.ijhydene.2023.09.008

Table 1 – Average Efficiency (E) after 10 redox cycles according to the redox condition and the sample type.

		E (%)					
	Sample	FeFOAM			FePOWD		
	Ethanol fed (*mmol*)	3.42	4.57	5.71	3.42	4.57	5.71
Temperature (°C)	675	12.03	21.10	40.42	6.16	7.44	11.84
	700	18.00	22.29	42.51	6.50	8.22	12.11
	750	30.51	51.71	73.96	9.98	11.75	62.58

Value underlined showed concentration of CO above 10 *ppm*.

Table 2 – Average Energy conversion efficiency (E_{energy}) after 10 redox cycles according to the redox condition and the sample type.

		E_{energy} (%)					
	Sample	FeFOAM			FePOWD		
	Ethanol fed (*mmol*)	3.42	4.57	5.71	3.42	4.57	5.71
Temperature (°C)	675	10.22	13.41	20.56	5.23	4.73	6.02
	700	15.29	14.17	21.62	5.52	5.22	6.16
	750	25.91	32.87	37.62	8.48	6.16	31.83

Value underlined showed concentration of CO above 10 *ppm*.

Table 3 – Summary of Fe-based oxygen carriers for SIP process.

Oxygen carrier	Reducing agent	T (°C)	Major results			
			H_2 yield *mmol* $H_2 \cdot g^{-1}_{sample}$	H_2 purity	Cycle	REF
Fe_2O_3/30 wt% Al_2O_3	CO	600	7.6	99.7	10	[24]
3 wt% Cu–Fe/MgAl	CH_4	900	1.1	98.5	10	[45]
75 wt% Fe_2O_3/Al_2O_3	CO	900	3.5	~100	20	[46]
$ZnFeAlO_4$	CO	850	2.2	~100	20	[47]
Fe_2O_3/La0.6Sr0.4Mg0.4Ga0.6O3-δ	CO	750	9.7	n.d.	100	[48]
15 mol% La-iron ore	CO	900	2.8	~100	10	[49]
$Mn_{0.5}Fe_{0.5}(FeAl)O_x$	CO	800	2.1	n.d.	20	[50]
FeFOAM (Fe_2O_3-2wt% Al_2O_3)	C_2H_5OH	750	5.1	~100	10	This work

n.d.: Not determined.

determination of the iron oxide reduction degree. However, these gas stream can be either purified [39] or used in extensively studied technologies with less stringent purity limits like production and annealing of steel [40,41] methanol or ammonia production. The average energy conversion efficiency (E_{energy}) of the each redox condition was also evaluated in terms of the combustion of the H_2 produced (LHV_{H_2}) per the ethanol used as fuel (LHV_{EtOH}) according to equation (18).

$$E_{energy}(\%) = \frac{LHV_{H2}\left(\frac{MJ}{kg}\right) \cdot H_{2produced}(kg)}{LHV_{EtOH}\left(\frac{MJ}{kg}\right) \cdot EtOH_{fed}(kg)} \cdot 100 \quad (18)$$

The comparison of the results obtained at each tested conditions are summarized in Table 2. Based on the results, the sample FeFOAM guarantee an enhanced energy recovery in the H_2 stream; the $E_{thenergy}(\%)$ values were always higher than FePOWD at each tested conditions. In the pure hydrogen production region, FeFOAM allows the highest $E_{energy}(\%)$ value of 26% at 750 °C and 3.42 *mmol* of ethanol fed, while only 8.5% was achieved at the same operative conditions with FePOWD.

From the comparison of the results with literature, the higher reactivity of FeFOAM is clearly demonstrated; In the research of Galvita et al. [42] the oxygen carrier 5 wt%Cr_2O_3-40 wt%Fe_2O_3–CeO_2–ZrO_2 presented good stability, but the maximum process efficiency was only 20%. Zhu et al. [43] achieved an efficiency value of 33% only feeding a mixture of 20 vol% of CH_4 in nitrogen for 40 min; Voitic et al. [44], produced a high purity hydrogen stream with an efficiency of 41%, feeding syngas for 90 *min* during the reduction step. On the contrary, FeFOAM was able to achieve a maximum efficiency of 30.51% with a reduction length of only 3 *min*, allowing not only to minimize the costs related to consumption of reducing agents but also to promote the scale up of the technology increasing the total rate of pure H_2 production. Furthermore, Table 3 summarized the major results reported in literature on Fe-based oxygen carriers under similar operational conditions.

Please cite this article as: Damizia M et al., Green hydrogen production using doped Fe_2O_3 foams, International Journal of Hydrogen Energy, https://doi.org/10.1016/j.ijhydene.2023.09.008

3.4. Post redox characterization of FeFOAM sample

The characterization of FeFOAM sample was performed on the sample subjected to the redox test at 750 °C, aiming at evaluating how pore structure, porosity, crystal phase, and atom distribution are enhanced by the increase of redox temperature. After redox test at 750 °C, the open porosity and the final density of the FeFOAM sample remains practically unchanged with no pore clogging. Fig. 7a shows the final pore structure with no significant modification as compare with Fig. 2b. However, the pores end up with a sponge-like surface (Fig. 7a) due to the progression of the redox reaction through the sample wall. In fact, a detail study on the sample surface

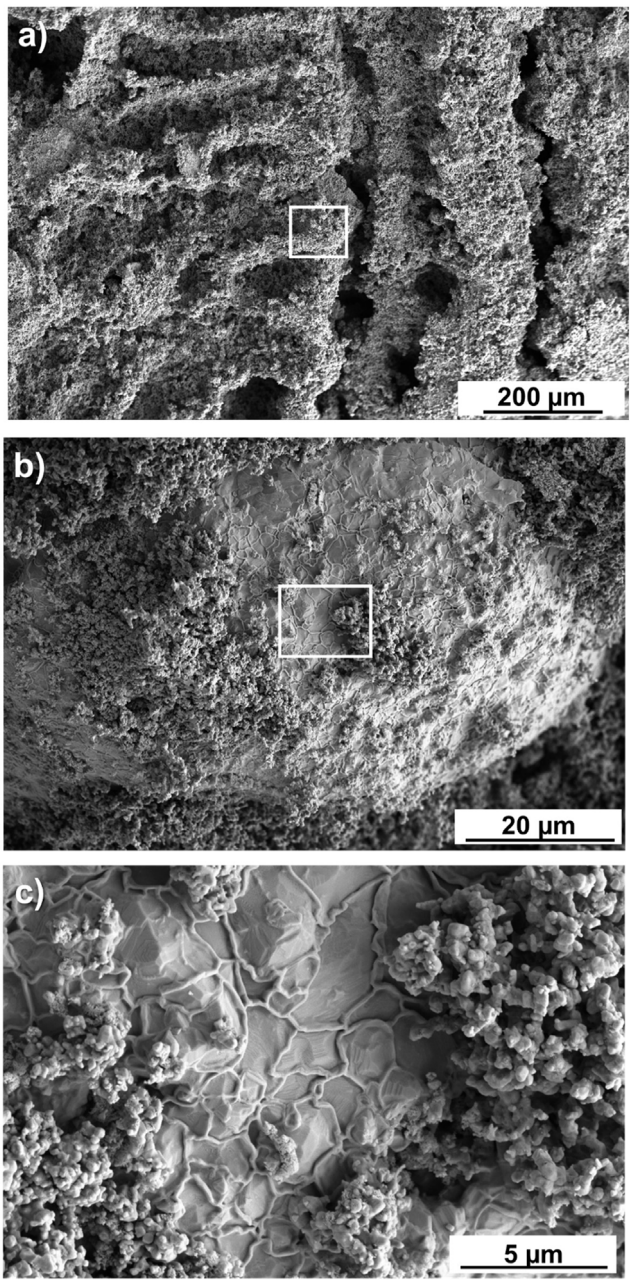

Fig. 7 – SEM images of the FeFOAM sample surface (a) after redox test at 750 °C. Higher magnification images (b, c) were taken at the corresponding square box.

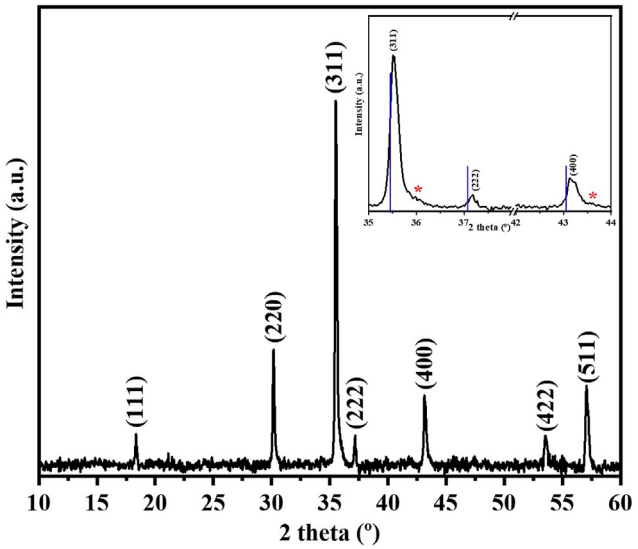

Fig. 8 – XRD pattern of the FeFOAM sample after redox test at 750 °C.

on Fig. 7b–c shows a spider-like network previously reported in the literature [51].

The XRD pattern for the FeFOAM sample (Fig. 8) shows the indexed peaks corresponding to the magnetite phase, i.e., the iron oxide with stoichiometry Fe_3O_4, face-centred cubic structure and Fd-3m Space Group Symmetry (ref. no 00-019-0629 in the PDF4+ database of the International Centre for Diffraction Data, ICDD). However, attending to the position of the peaks, it is detected a displacement of all peaks to higher diffraction angle or lower interplanar distance and, consequently, lower lattice parameters (see inset in Fig. 8). This effect can be attributable to the introduction of Al cations into the Fe_3O_4 crystalline structure. Due to the lower cationic radius of Al^{3+} (57 *pm*) than Fe^{2+} (82 *pm*) and Fe^{3+} (67 *pm*), by the substitution of Al^{3+} by Fe^{3+} it is expected to generate a higher 2 theta degree displacements, such as it occurs. The total absence of peaks of Al or Al_2O_3 phase are in consonance with this assertion. Finally, two small peaks can be detected close to the (311) and (400) peaks from the Fe_3O_4. Those peaks, marked as an asterisk in the inset of Fig. 8, are even more shifted to higher 2 theta degree than the majority solid solution $(Fe_xAl_{1-x})_3O_4$, suggests a higher Al content in that case. Therefore, after 10 redox cycles the Al cations added during the powder synthesis remained in a solid solution and no Fe_2AlO_4 spinel phase was formed.

Furthermore, a TEM study was carried out to fully characterized the element distribution in the FeFOAM sample after the redox cycles. In Fig. 9a corresponding to EDS-HAADF-TEM images can be observed an optimal distribution of Fe and O, and an acceptable distribution of Al at the particles of the FeFOAM. This aspect could indicate the formation of the $(Fe,Al)_3O_4$ solid solution magnethite. In addition, in some area of the particles, the Al ratio seems to be higher than the general aspect (marked with dotted square in Fig. 9a), probably as consequence of higher Al composition of this particle in the Fe/Al ratio of the $(Fe,Al)_3O_4$. In addition, the measurements of HRTEM images show the evident crystallographic

Please cite this article as: Damizia M et al., Green hydrogen production using doped Fe_2O_3 foams, International Journal of Hydrogen Energy, https://doi.org/10.1016/j.ijhydene.2023.09.008

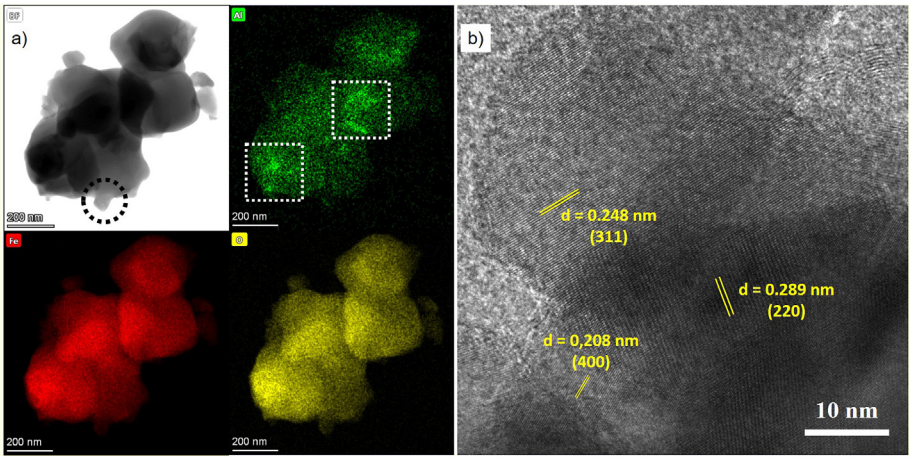

Fig. 9 – EDS-HAADF-TEM images of FeFOAM sample after redox test at 750 °C, atom distribution (a) and crystallographic planes (b).

planes for the Fe_3O_4 magnethite phase. As example, in Fig. 9b is presented the HRTEM images selected in the area marked as dotted circle in Fig. 9a, showing the (220), (311) and (400) crystallographic planes. In addition, the interplanar distance of these planes are diminished in comparison with the corresponding to the Fe_3O_4, face-centred cubic structure. Concretely, 0.289 nm *vs* 0.297 *nm* for (220), 0.248 *nm vs* 0.253 *nm* for (311) and 0.208 *nm vs* 0.210 *nm* for (400), respectively.

It seems that limiting the degreed of conversion of the oxygen carriers, not only avoid the introduction of *CO* at the hydrogen stream, but also prevent the atom migration of Fe reported by Sun et al. [52] and Saito et al. [26]. Another aspect is the sintering temperature of 1100 °*C* used to manufactured the foams, according to Ma et al. [53] lower calcination temperature contribute to prevent phase segregation by the higher content of surface lattice oxygen in the oxygen carrier. In this work, particle synthesis was performed at 620 °*C* to mitigate particle growth and to enhance the particle sintering during foam manufacturing.

4. Conclusions

This work has successfully manufactured hematite foams suitable for high purity hydrogen production. The foams showed a higher level of hydrogen production with a sufficient process efficiency to become a viable solution to mass-produces H_2. This behaviour was based on a combination of factors like: Low calcination temperature during powder synthesis, which guaranties a much homogeneous Al atom distribution, preventing further sintering process during redox cycling. Sufficient active surfaces created by freeze-casting method, ensuring high interconnected porosity with no pressure-drop. The created porosity (i.e. the pore size) guaranties enough distance between the pore surface to prevent pore clogging by accommodate the volumetric expansion of the oxide layer regrowing during the sequential oxidation steps.

The production of high yields of pure hydrogen from bio-ethanol suitable for the direct use in PEMFC was always enhanced using the foam. The maximum yield was achieved at 750 °*C* with a reduction time of 3 *min*, where FeFOAM produced approximately 5.1 $mmol\ H_2 \cdot g^{-1}_{sample}$ of highly pure H_2 (<10 *ppm CO*) per gram of sample and millilitre of ethanol fed in each redox cycle. Furthermore, no deactivation in H_2 production was detected demonstrating that the presence of 2 wt % of Al_2O_3 confers an excellent thermal resistance during thermal cycling, guaranteeing the stable production of high purity H_2 yields for 10 consecutive redox cycle with both the samples.

Declaration of competing interest

The authors declare that they have no known competing financial interests or personal relationships that could have appeared to influence the work reported in this paper.

Acknowledgments

Financial support for this work has been provided by: Grant PID2021-123010OB-I00 funded by MCIN/AEI/10.13039/501100011033 and by "ERDF A way of making Europe". Grant TED2021-129920B–C41–C42–C43–C44 funded by MCIN/AEI/10.13039/501100011033 and by the "European Union NextGenerationEU/PRTR".

REFERENCES

[1] Nikolaidis P, Poullikkas A. A comparative overview of hydrogen production processes. Renew Sustain Energy Rev 2017;67:597–611. https://doi.org/10.1016/j.rser.2016.09.044.
[2] Karayel GK, Javani N, Dincer I. Green hydrogen production potential for Turkey with solar energy. Int J Hydrogen Energy 2022;47:19354–64. https://doi.org/10.1016/j.ijhydene.2021.10.240.
[3] Boretti A. Production of hydrogen for export from wind and solar energy, natural gas, and coal in Australia. Int J

Hydrogen Energy 2020;45:3899–904. https://doi.org/10.1016/j.ijhydene.2019.12.080.
[4] Pinsky R, Sabharwall P, Hartvigsen J, O'Brien J. Comparative review of hydrogen production technologies for nuclear hybrid energy systems. Prog Nucl Energy 2020;123:103317. https://doi.org/10.1016/j.pnucene.2020.103317.
[5] De Filippis P, D'Alvia L, Damizia M, Caprariis B, Del Prete Z. Pure hydrogen production by steam-iron process: the synergic effect of MnO2 and Fe2O3. Int J Energy Res 2021;45:4479–94. https://doi.org/10.1002/er.6117.
[6] Thaler M, Hacker V. Storage and separation of hydrogen with the metal steam process. Int J Hydrogen Energy 2012;37:2800–6. https://doi.org/10.1016/j.ijhydene.2011.06.119.
[7] Zhang D, Duan R, Li H, Yang Q, Zhou H. Optimal design, thermodynamic, cost and CO2 emission analyses of coal-to-methanol process integrated with chemical looping air separation and hydrogen technology. Energy 2020;203. https://doi.org/10.1016/j.energy.2020.117876.
[8] Durán P, Lachén J, Plou J, Sepúlveda R, Herguido J, Peña JA. Behaviour of freeze-casting iron oxide for purifying hydrogen streams by steam-iron process. Int J Hydrogen Energy 2016;41:19518–24. https://doi.org/10.1016/j.ijhydene.2016.06.062.
[9] de Caprariis B, Damizia M, De Filippis P, Bracciale MP. The role of Al2O3, MgO and CeO2 addition on steam iron process stability to produce pure and renewable hydrogen. Int J Hydrogen Energy 2021;46:39067–78. https://doi.org/10.1016/J.IJHYDENE.2021.09.135.
[10] Vuppaladadiyam AK, Vuppaladadiyam SSV, Awasthi A, Sahoo A, Rehman S, Pant KK, et al. Biomass pyrolysis: a review on recent advancements and green hydrogen production. Bioresour Technol 2022;364:128087. https://doi.org/10.1016/j.biortech.2022.128087.
[11] Hedayati A, Soleimanisalim AH, Mattisson T, Lyngfelt A. Thermochemical conversion of biomass volatiles via chemical looping: comparison of ilmenite and steel converter waste materials as oxygen carriers. Fuel 2022;313:122638. https://doi.org/10.1016/j.fuel.2021.122638.
[12] Ma Y, Wang XR, Li T, Zhang J, Gao J, Sun ZY. Hydrogen and ethanol: production, storage, and transportation. Int J Hydrogen Energy 2021;46:27330–48. https://doi.org/10.1016/j.ijhydene.2021.06.027.
[13] Chang W, Hu Y, Xu W, Huang C, Chen H, He J, et al. Recent advances of oxygen carriers for hydrogen production via chemical looping water-splitting. Catalysts 2023;13. https://doi.org/10.3390/catal13020279.
[14] Ma Z, Zhang S, Xiao R. Insights into the relationship between microstructural evolution and deactivation of Al2O3 supported Fe2O3 oxygen carrier in chemical looping combustion. Energy Convers Manag 2019;188:429–37. https://doi.org/10.1016/j.enconman.2019.03.073.
[15] Yan J, Shen T, Wang P, Yin X, Zhu X, Jiang S, et al. Redox performance of manganese ore in a fluidized bed thermogravimetric analyzer for chemical looping combustion. Fuel 2021;295:120564. https://doi.org/10.1016/j.fuel.2021.120564.
[16] Li K, Haneda M, Gu Z, Wang H, Ozawa M. Modification of CeO2 on the redox property of Fe 2O3. Mater Lett 2013;93:129–32. https://doi.org/10.1016/j.matlet.2012.09.039.
[17] Zeng D, Qiu Y, Zhang S, Ma L, Li M, Cui D, et al. Synergistic effects of binary oxygen carriers during chemical looping hydrogen production. Int J Hydrogen Energy 2019;44:21290–302. https://doi.org/10.1016/j.ijhydene.2019.06.118.
[18] Ricca A, Truda L, Palma V. Study of the role of chemical support and structured carrier on the CO2 methanation reaction. Chem Eng J 2019;377:120461. https://doi.org/10.1016/j.cej.2018.11.159.
[19] Portela R, Wolf P, Marinkovic JM, Serrano-Lotina A, Riisager A, Haumann M. Tailored monolith supports for improved ultra-low temperature water-gas shift reaction. React Chem Eng 2021;6:2114–24. https://doi.org/10.1039/D1RE00226K.
[20] Klenov OP, Chumakova NA, Pokrovskaya SA, Noskov AS. Modeling of heat transfer in a porous monolith catalyst with square channels. Ind Eng Chem Res 2016;55:3879–89. https://doi.org/10.1021/acs.iecr.5b04804.
[21] Tuci G, Liu Y, Rossin A, Guo X, Pham C, Giambastiani G, et al. Porous silicon carbide (SiC): a chance for improving catalysts or just another active-phase carrier? Chem Rev 2021;121:10559–665. https://doi.org/10.1021/acs.chemrev.1c00269.
[22] Wilke SK, Dunand DC. Structural evolution of directionally freeze-cast iron foams during oxidation/reduction cycles. Acta Mater 2019;162:90–102. https://doi.org/10.1016/j.actamat.2018.09.054.
[23] Long Y, Li K, Gu Z, Zhu X, Wei Y, Lu C, et al. Ce-Fe-Zr-O/MgO coated monolithic oxygen carriers for chemical looping reforming of methane to co-produce syngas and H2. Chem Eng J 2020;388:124190. https://doi.org/10.1016/j.cej.2020.124190.
[24] Chang Y, Li G, Ma S, Zhao X, Li N, Zhou X, et al. Effect of hierarchical pore structure of oxygen carrier on the performance of biomass chemical looping hydrogen generation. Energy 2022;254:124301. https://doi.org/10.1016/j.energy.2022.124301.
[25] Ma Z, Lu Y, Liu G. Enhanced cyclic redox reactivity of Fe2O3/Al2O3 by Sr doping for Chemical-Looping combustion of solid fuels. Fuel 2022;324:124625. https://doi.org/10.1016/j.fuel.2022.124625.
[26] Saito Y, Kosaka F, Kikuchi N, Hatano H, Otomo J. Evaluation of microstructural changes and performance degradation in iron-based oxygen carriers during redox cycling for chemical looping systems with image analysis. Ind Eng Chem Res 2018;57:5529–38. https://doi.org/10.1021/acs.iecr.7b04966.
[27] Ma Z, Wu K, Wang H, Zhu L, Li Z, Luo Y, et al. Mechanism of solid state diffusion on the performance evolution of iron-based oxygen carrier at different operating conditions for chemical looping process. Fuel 2023;331:125699. https://doi.org/10.1016/j.fuel.2022.125699.
[28] Fumoto E, Sato S, Takanohashi T. Characterization of an iron-oxide-based catalyst used for catalytic cracking of heavy oil with steam. Energy Fuels 2018;32:2834–9. https://doi.org/10.1021/acs.energyfuels.8b00054.
[29] De Vos Y, Jacobs M, Van Der Voort P, Van Driessche I, Snijkers F, Verberckmoes A. Sustainable iron-based oxygen carriers for chemical looping for hydrogen generation. Int J Hydrogen Energy 2019;44:1374–91. https://doi.org/10.1016/j.ijhydene.2018.11.099.
[30] Lloreda-Jurado PJ, Balu K, Hernández-Saz J, Chicardi E, Ferrari B, Sepúlveda R. Alumina doped Fe2O3 foams by freeze-casting for redox cycling applications. J Eur Ceram Soc 2022;42:5922–31. https://doi.org/10.1016/j.jeurceramsoc.2022.06.054.
[31] Lloreda-Jurado PJ, Perez-Puyana V, Romero A, Sepúlveda R. Influences of the solid load on the microstructure and compressive behavior of Fe2O3 scaffolds manufactured by freeze-casting using stearic acid as dispersant agent. J Eur Ceram Soc 2022;42:193–201. https://doi.org/10.1016/j.jeurceramsoc.2021.09.056.
[32] Damizia M, Bracciale MP, Anania F, Tai L, De Filippis P, de Caprariis B. Efficient utilization of Al2O3 as structural promoter of Fe into 2 and 3 steps chemical looping hydrogen

Please cite this article as: Damizia M et al., Green hydrogen production using doped Fe_2O_3 foams, International Journal of Hydrogen Energy, https://doi.org/10.1016/j.ijhydene.2023.09.008

process: pure H2 production from ethanol. Int J Hydrogen Energy 2023. https://doi.org/10.1016/j.ijhydene.2023.04.067.
[33] Kim Y, Lim HS, Kim HS, Lee M, Lee JW, Kang D. Carbon dioxide splitting and hydrogen production using a chemical looping concept: a review. J CO2 Util 2022;63:102139. https://doi.org/10.1016/j.jcou.2022.102139.
[34] Wilke SK, Lundberg RA, Dunand DC. Hierarchical structural changes during redox cycling of Fe-based lamellar foams containing YSZ, CeO_2, or ZrO_2. ACS Appl Mater Interfaces 2020;12:27190–201. https://doi.org/10.1021/acsami.0c05107.
[35] Lloreda-Jurado PJ, Wilke SK, Scotti K, Paúl-Escolano A, Dunand DC, Sepúlveda R. Structure–processing relationships of freeze-cast iron foams fabricated with various solidification rates and post-casting heat treatment. J Mater Res 2020:1–10. https://doi.org/10.1557/jmr.2020.175.
[36] Trevisanut C, Mari M, Millet J-MM, Cavani F. Chemical-loop reforming of ethanol over metal ferrites: an analysis of structural features affecting reactivity. Int J Hydrogen Energy 2015;40:5264–71. https://doi.org/10.1016/j.ijhydene.2015.01.054.
[37] Zeng P, Dou B, Zhang H, Wu K, Zhao L, Luo C, et al. Chemical looping steam reforming of ethanol without and with in-situ CO2 capture. Int J Hydrogen Energy 2022;47:6552–68. https://doi.org/10.1016/j.ijhydene.2021.12.066.
[38] Jiang B, Dou B, Wang K, Zhang C, Song Y, Chen H, et al. Hydrogen production by chemical looping steam reforming of ethanol using NiO/montmorillonite oxygen carriers in a fixed-bed reactor. Chem Eng J 2016;298:96–106. https://doi.org/10.1016/j.cej.2016.04.027.
[39] Kumabe K, Hasegawa Y, Moritomi H. Effect of hydrogen separation on coal char gasification with subcritical steam using a calcium-based CO_2 sorbent. ACS Omega 2020;5:236–42. https://doi.org/10.1021/acsomega.9b02591.
[40] Abdul Quader M, Ahmed S, Dawal SZ, Nukman Y. Present needs, recent progress and future trends of energy-efficient Ultra-Low Carbon Dioxide (CO2) Steelmaking (ULCOS) program. Renew Sustain Energy Rev 2016;55:537–49. https://doi.org/10.1016/j.rser.2015.10.101.
[41] Wang RR, Zhao YQ, Babich A, Senk D, Fan XY. Hydrogen direct reduction (H-DR) in steel industry—an overview of challenges and opportunities. J Clean Prod 2021;329:129797. https://doi.org/10.1016/j.jclepro.2021.129797.
[42] Galvita V, Sundmacher K. Cyclic water gas shift reactor (CWGS) for carbon monoxide removal from hydrogen feed gas for PEM fuel cells. Chem Eng J 2007;134:168–74. https://doi.org/10.1016/j.cej.2007.03.046.
[43] Zhu M, Song Y, Chen S, Li M, Zhang L, Xiang W. Chemical looping dry reforming of methane with hydrogen generation on Fe2O3/Al2O3 oxygen carrier. Chem Eng J 2019;368:812–23. https://doi.org/10.1016/j.cej.2019.02.197.
[44] Voitic G, Nestl S, Malli K, Wagner J, Bitschnau B, Mautner F-A, et al. High purity pressurised hydrogen production from syngas by the steam-iron process. RSC Adv 2016;6:53533–41. https://doi.org/10.1039/C6RA06134F.
[45] Hu J, Chen S, Ni Xiang W. Co and Cu-promoted iron-based oxygen carriers in methane-fueled chemical looping hydrogen generation process. Fuel Process Technol 2021;221:106917. https://doi.org/10.1016/j.fuproc.2021.106917.
[46] Qiu Y, Zeng D, Chen C, Zeng J, Zhang S, Xiao R. Performance of oxygen carriers with different porosities in chemical looping water-splitting. Energy Technol 2018;6:1723–31. https://doi.org/10.1002/ente.201800135.
[47] Cui D, Li M, Qiu Y, Ma L, Zeng D, Xiao R. Improved hydrogen production with 100% fuel conversion through the redox cycle of ZnFeAlOx oxygen carrier in chemical looping scheme. Chem Eng J 2020;400:125769. https://doi.org/10.1016/j.cej.2020.125769.
[48] He H, Jiang H, Yang F, Zhang W, Jin M, Li Z. Sr, Mg co-doped LaGaO3-δ supported Fe2O3 improved the water gas shift reaction with chemical looping. Int J Hydrogen Energy 2023;48:1263–76. https://doi.org/10.1016/j.ijhydene.2022.10.018.
[49] Gu H, Cui X, Wang J, Li W, Wu X, Wang L, et al. Natural iron ore as oxygen carrier modified with rare earth metal for chemical looping hydrogen production. Energy Fuels 2021;35:15234–42. https://doi.org/10.1021/acs.energyfuels.1c02105.
[50] Zeng D, Cui D, Qiu Y, Li M, Ma L, Zhang S, et al. Mn-Fe-Al-O mixed spinel oxides as oxygen carrier for chemical looping hydrogen production with CO2 capture. Fuel 2020;274:117854. https://doi.org/10.1016/j.fuel.2020.117854.
[51] Lloreda-Jurado PJ, Hernández-Saz J, Chicardi E, Paúl A, Sepúlveda R. Pore morphology evolution and atom distribution of doped Fe2O3 foams developed by freeze-casting after redox cycling. J Mater Res Technol 2021;13:1887–98. https://doi.org/10.1016/j.jmrt.2021.06.008.
[52] Sun Z, Zhou Q, Fan L-S. Formation of core–shell structured composite microparticles via cyclic gas–solid reactions. Langmuir 2013;29:12520–9. https://doi.org/10.1021/la4029832.
[53] Ma Z, Liu G, Lu Y, Zhang H. Redox performance of Fe2O3/Al2O3 oxygen carrier calcined at different temperature in chemical looping process. Fuel 2022;310:122381. https://doi.org/10.1016/j.fuel.2021.122381.

Please cite this article as: Damizia M et al., Green hydrogen production using doped Fe_2O_3 foams, International Journal of Hydrogen Energy, https://doi.org/10.1016/j.ijhydene.2023.09.008